Zinc oxide Nanoparticles as Contrast Enhancing Agents for Microwave Imaging

Rachita Lahri,* Mohammed W.Rahman,* Micheal J.Wright,* Panagiotis Kosmas,† and Maria Thanou‡

(Dated: April 27, 2018)

Abstract

Purpose: Microwave imaging/sensing is an emerging technology that shows potential for healthcare diagnostic applications, particularly in breast cancer detection. This technique estimates the anatomically variant dielectric properties of the breast. Similar to other imaging modalities, nanoparticles (NPs) could potentially be utilised as contrast agents to increase contrast between healthy and malignant tissues.

Methods: In this study, aqueous suspensions of NPs such as surface modified single walled carbon nanotubes, zinc oxide, and silicon dioxide are studied to assess their potential effective contrast for microwave imaging. Morphology characterisation of the NPs have been achieved using atomic force microscopy (AFM) and scanning electron microscopy (SEM). The size and stability of colloidal dispersions have been characterised by dynamic light scattering technique (DLS) and Ultraviolet-visible spectrophotometry (UV-Vis). The dielectric characterisation of the aqueous based colloidal suspensions is recorded over the microwave frequency range between 1–4 GHz.

Results: Zinc oxide NP dispersion has shown an increase in the dielectric constant compared to the background medium. Furthermore, PEGylation of ZnO NPs can achieve a valid increase in the dielectric constant compared to water, which was shown to be concentration dependent.

Conclusion: These results suggest that ZnO nanomaterials have the potential to be used in biomedical applications such as breast imaging to improve diagnostic capabilities.

* Faculty of Life Sciences & Medicine, King's College London, Waterloo, London, United Kingdom SE1 9NH

† Faculty of Natural & Mathematical Sciences, King's College London, Strand, London, United Kingdom WC2R 2LS

‡ Faculty of Life Sciences & Medicine, King's College London, Waterloo, London, United Kingdom SE1 9NH ; Author to whom correspondence should be addressed. E-mail: maria.thanou@kcl.ac.uk

I. INTRODUCTION

Microwave imaging (MWI) is a novel imaging modality that offers several desirable characteristics for breast cancer detection and other diagnostic applications[1]. This method is attractive because it's regarded safe, as it relies on non-ionising electromagnetic radiation, avoids breast compression, can provide real time imaging and has the potential for personalised treatment through microwave hyperthermia[2, 3]. At microwave frequencies, biological tissues exhibit distinct electrical properties, due to different percentage of water content, which is an important factor in determining the dielectric constant. Low water content tissues such as adipose ($\epsilon'(\omega) = 5.4$) will have a lower dielectric constant than high water content tissue such as skin ($\epsilon'(\omega) = 40.9$) or muscle ($\epsilon'(\omega) = 54.8$)[4]. The variation in dielectric properties observed between healthy, fibro-glandular and cancer tissues may be associated with the tendency of certain cancer tissues possessing a higher water content and sodium ion concentration. The electrochemical properties of the cancer cell membranes may also differ from normal cells[5].

Various tissue studies have attempted tissue characterisation to relate dielectric properties to its physiological state (healthy or diseased). In early studies, Joines *et al.*[6] analysed 24 normal and malignant breast tissues samples. The dielectric properties of malignant tissues were approximately 200–500 % greater than the dielectric properties of normal tissues at 900 MHz. More recently, a series of *ex vivo* studies carried out by Lazebnik *et al.*[7] characterised the broadband electrical properties (0.5–20 GHz) of diverse breast tissue types, taken from breast reduction surgeries on a large sample population. The results showed that dielectric properties were determined by the percentage content of adipose (fat) in each sample and that other factors such as age, and tissue temperature variability were negligible. The second segment of the large scale study from cancer surgeries by Lazebnik *et al.*[8] reports the dielectric characterisation of normal, benign and malignant tissue samples. Contrast between malignant and fatty breast tissues may be as large as 10:1, however distinction between malignant and healthy fibro-glandular tissues can be as low as 10 %.

These results suggest that chemical entities/NPs may be necessary to enhance the dielectric constant further and avoid false negative values in clinical assessments. NPs can accumulate in tumours passively via the enhanced permeation and retention effect (EPR)[9]. EPR is the result of the tumour's leaky vasculature and poorly developed lymphatic system.

In particular, angiogenic vessels have large pore size up to 200nm. Due to these pores, NPs extravasate in tumours more than they do in healthy tissues.

Various studies have been conducted to evaluate the impact of well-known NPs in the microwave frequency range. Ogunlade *et al.*[10] measured superparamagnetic carboxydextran coated iron oxide NPs and single-walled carbon nanotubes (SWCNTs) with PL-PEG-NH_2 (Phospholipid-PEG-Amine) as a dispersant at 3 GHz using a cavity perturbation technique, and were found to have a negligible contrast. Gadolinium based contrast agents were also characterised using the same technique. Li *et al.*[11] reported that SWCNTs (0.5 μm in length) dispersed in water with 1 % (v/v) Pluronic surfactant at concentrations of 0.5 & 1 mg/mL increased the dielectric properties compared to the background medium. In the same study, dielectric properties of PL-PEG functionalised SWCNTs (synthesized by commercial High-pressure CO conversion; Unidym, Inc.) at a concentration of 2 mg/mL were measured from 0.5–10 GHz and were clearly shown to have a 90 % increase in the effective conductivity and 10 % in dielectric constant compared to the properties of PL-PEG in water at 1 GHz. Li *et al.* also studied the dispersion consisting of 30 % volume fraction of copper NPs (384 nm) in ethylene glycol. The dielectric constant was 20 % higher than that of pure ethylene glycol but negligible change in effective conductivity was observed. They also characterised, spherical and rod shaped gold NPs (synthesized using an aqueous seeded method with an average diameter of 20 nm) coated with Cetrimonium bromide (CTAB), but insignificant change was observed compared to the background medium.

Xie *et al.*[12] demonstrated that carbon nanotubes (CNTs) (50:50 ratio of single and double walled synthesized by chemical vapour deposition) which had been functionalized via H_2SO_4:HNO_3 treatment with vigorous sonication may have a stable dispersion at higher concentrations. Dielectric properties of 10 & 20 mg/mL concentrations of CNTs dispersed in a mixture of deionised water and mannitol (50 mg/mL) in the frequency range of 0.5–6 GHz were measured and results showed enhanced dielectric properties. Successful functionalization of CNTs with carboxylic and sulfonic groups after acid treatment on the outer CNT walls was responsible for the increased dispersion, and colloidal stability was attributed to the stronger length-shortening effect. Xie *et al.*[13] carried out acid purification methods (Hydrochloric acid/Hydrogen peroxide method and Nitric acid reflux method) for modifying single walled carbon nanotubes (Co-SWCNTs synthesized by catalytic chemical vapour deposition, and Fe-SWCNTs synthesized by high pressure CO method) and their dielectric

properties were studied using a slim form probe between 0.5–6 GHz. For microwave frequency dielectric measurements, 3 mg/mL of SWCNTs were dispersed in 0.1 % aqueous PL-PEG$_{5400}$-NH$_2$ (Phospholipid-Polyethyleneglycol-Amine) or DSPE-PEG (1, 2-Distearoyl-sn-glycero-3-phosphoethanolamine-Polyethyleneglycol) and sonicated for 12 hours. Results showed there is a large increase in the dielectric properties for pristine Co-SWCNT compared to the control (CNT free solution). At 3 GHz, pristine Co-SWCNT showed a 10 % increase in the dielectric constant and 40 % increase in the effective conductivity compared to the control. Similar trends were observed for pristine Fe-SWCNT compared to the control. Both acid purification methods were shown to decrease the dielectric properties for both Co-SWCNT and Fe-SWCNT. This indicates that disruption of the pristine structure of CNTs may have an undesirable effect on their use as microwave contrast enhancement agents.

Mashal *et al.*[14] measured the dielectric properties of SWCNTs (with a diameter of 1–2 nm and 5–30 μm in length obtained from Cheaptubes, Inc.) dispersed in tissue mimicking materials. A 10 % oil-in-gel phantoms with various concentrations of SWCNTs (1, 2, and 3 mg/mL) in 1 % by weight mixture of Pluronic were prepared. Dielectric properties were measured over a frequency range of 0.6–20 GHz. The average dielectric constant of a pure phantom and phantoms with 1, 2, and 3 mg/mL of SWCNTs was 53.3, 57.9, 63.7 and 77.3 respectively, therefore not only showing contrast from the background but also a contrast increase with an increase in NP concentration. Another study by Mashal *et al.*[15] investigated the use of air-filled microbubbles (average diameter of 18 μm and density of 0.6 g mL^{-1}) as potential contrast agents. Mixtures of ethylene glycol with 0–30 % weight concentrations were characterised. The dielectric properties decreased with an increase in microbubble concentration at 3 GHz.

Magnetic iron oxide NPs have been studied for their potential to produce magnetic contrast in a novel microwave detection system [16, 17]. The electrical and magnetic properties of this magnetite suspension have been accurately characterised using a custom-designed transmission line method[18, 19], which uses both forward transmission and return loss parameters in approximating the properties(S_{11} and S_{21}). The advantage of using magnetic NPs is that they can be functionalised by molecules such as peptides or antibodies, which can then bind to the receptors of cancer cells. The magnetic NPs are biocompatible, hence could be intravenously administered.

Additional studies are required to identify promising and safe contrast enhancement agents for MWI. It is possible that conductive and semi-conductive materials may present certain physical properties that affect the dielectric properties of a medium. Therefore, we decided to study other NPs in water to suggest alternatives as potential contrast agents for MWI. SiO_2 suspensions are characterised to act as a negative control, as SiO_2 NPs structure does not demonstrate any potential of being a contrast agent. Carbon nanotubes have been previously shown to have a viable microwave contrast for breast imaging. Therefore, CNTs are used as controls to compare the dielectric contrast obtained from ZnO, SiO_2 and ZnO-PEG in colloidal dispersions.

To this end, we have shown that zinc oxide NPs modified using different molecular weights of a stabilising agent (polyethylene glycol) will affect the stability and size of the NPs[20]. The notable differences in the dielectric contrast of colloidal dispersions due to ZnO-PEG is the main contribution of the paper, as evidenced by our dielectric spectroscopy measurements in the frequency range of 1-4 GHz. Besides presenting a new promising contrast agent for MWI, the paper offers some insight on the physicochemical properties, which are not deeply studied in previous literature on contrast agents for MWI.

II. MATERIALS

The materials used in this study are as follows; zinc oxide (Sigma-Aldrich Company Ltd; Stated manufacturer size of <100 nm), silicon dioxide - quartz, (Sigma-Aldrich Company Ltd; Stated manufacturer size of 10-20 nm), polyethylene glycol (Sigma-Aldrich Company Ltd; average molecular weight (M_W) of 8000 Da), Pluronic F–127 (Sigma-Aldrich Company Ltd) and CNT-OH (Cheaptubes, Inc.; Stated manufacturer size of 1–4 nm in diameter and 5-30 μm in length; >90 % purity; 3.9 % OH groups used, as they have better dispersion properties).

III. METHODS

A. Morphological characterisation of nanoparticles

Morphological studies provide detailed surface data of NPs. Topographical, morphological and compositional information regarding the surface of a sample is obtained from

SEM and AFM. The information obtained from these microscopies may indicate the particle diameter and its shape in its normal physical state.

1. Atomic force microscopy (AFM)

Prior to imaging, 1 mg/mL solution of the NPs were sonicated and a small amount is pipetted onto a mica sheet (10 mm x 10 mm) and dried using nitrogen gas. Images were taken using the Bruker icon dimension atomic force microscope, with the standard tapping mode applied. The scanning area started at a region of 10 μm x 10 μm, and is decreased to a smaller region of interest (ROI) of 1.66 μm x 1.66 μm. The scan rate decreased from 0.99–0.70 Hz as the scan size decreased, to improve image quality. The software uses a PID feedback system to improve the trace and retrace signals. To improve the reliability of image acquisition, the scan angle of the probe is altered from 0° to 90° and the raster scan for the images is repeated. This is a confidence check to observe any artefacts produced because of particles/dust stuck onto the cantilever.

2. Scanning electron microscopy (SEM)

For sample preparation, 2 mg/mL concentration for each nanoparticle was prepared; 100 μL of the suspension was pipetted onto a glass microscopic slide and was dried using nitrogen gas. The glass slide was coated with an electrically conducting layer of gold. Coating is crucial as it prevents charging of the specimen, which would otherwise occur due to accumulation of static electric field. SEM images were taken using a Hitachi scanning electron microscope with EDX elemental analysis (Oxford instruments) which has a resolution of $\sim$ 10 nm at 25 kV and 80 kX magnification.

B. Turbidity measurement using ultraviolet-visible spectrophotometry (UV-Vis)

A spectrophotometer was used to measure the turbidity of our samples. A spectrophotometer measures the amount of light that can pass through a solution. It is apparent that less light would pass through a solution which is more turbid or is a coloured solution. This technique was used to measure the stability of the dispersion of NPs in water over a time

period of 4 hours, with a sample population of 6 elements. Absorption or transmission measurements were taken by the S2000 UV/Vis Spectrophotometer. ZnO and ZnO-PEG were suspended in aqueous solution at a concentration of 1 mg/mL and serially diluted to 20 μg/mL. The suspensions were sonicated for 60 min and vortex shaken at 10 min intervals and measurements of light transmission were taken at a wavelength (λ) of 415 nm.

C. Nanoparticle size measurement using dynamic light scattering (DLS)

Dynamic light scattering is a technique which records the averaged intensity weighted particle diameter of the NPs in a suspension. As the dielectric measurements are performed in suspensions, it was crucial to understand the macroscopic and microscopic particle interactions when in solution compared to their physical state. Colloidal suspensions were prepared at a final concentration of 20 μg/mL, which was chosen as optimal, because lower concentrations would show increased baseline fluctuations and a higher intercept in the correlation function. Measurements were carried out on five set of samples for each NP with a 2 min equilibration time, taken at 25°C over a period of 4h, with a sample population of 6 elements. DLS was carried out using the Malvern Zetasizer Nano S, which provides the Cumulants analysis; Z-average size (nm) and polydispersity index (dimensionless).

D. ZnO nanoparticle surface modification using PEG

750 mg of PEG ((M_W) = 8000 Da) stirred into 100 mL of Reverse osmosis (RO) purified water until it was completely dissolved. 606.9 mg (15 mg/mL) of zinc oxide powder was suspended into 40 mL of RO water and sonicated (f = 37 kHz, P = 160 W) vigorously for 1h, and vortex shaken at 20 mins intervals. The pH of the solution was adjusted to be 8.5 by adding 0.05 M sodium hydroxide (NaOH) followed by 30 mins of stirring and a following 30 mins of sonication. 10 mL of the PEG solution was added to the ZnO NPs suspension followed by a final 1h of sonication. The reaction mixture was stirred for 48h at room temperature. The NPs were collected in a centrifuge and washed in water, followed by further washing procedure, to remove unabsorbed polymer. The powder was dried overnight under high vaccum[21].

E. Sample preparation for dielectric characterisation

Dispersions of 2, 1, 0.5, and 0.25 mg/mL for each nanomaterial (CNT-OH, SiO_2, ZnO, and ZnO-PEG) were prepared. We have studied lower concentrations of NPs to observe the minimum amount of nanomaterial needed to cause a difference in microwave dielectric properties in a simple background medium, such as water. 2 mg/mL was chosen as the highest concentration for this study. At 2 mg/mL aggregation of the NPs was observed and concentrations higher than that would have aggregated even further, which would have affected the microwave dielectric properties.Colloidal dispersions were made in a final volume of 20 mL with 1 % (v/v) Pluronic F–127. It is a non-ionic triblock copolymer composed of a central hydrophobic chain of polyoxypropylene with two hydrophilic chains of polyoxyethylene. Pluronic is known to have high solubility in water. The surfactant was used to improve the dispersion of NPs in water. Pluronic 1 % (v/v) has been added to SiO_2 and non-PEGylated ZnO NPs to improve their dispersion in order to be able to perform measurements. Without surfactant these particles sediment. We have not added 1 % (v/v) Pluronic in CNT-OH and ZnO-PEG, as they are modified to be dispersed.

F. Characterisation of dielectric properties

Dielectric characterisation was recorded using a commercial open-ended coaxial cable method[22]. The slim-form probe was calibrated using three known dielectric materials; air, short block (conductive elastomer that mimics electrical properties of metal), and RO water. Our lab is internally temperature controlled. Three different samples for each NP were prepared and 10 set of measurements were taken over different days to understand the repeatability better. The minimum and maximum frequencies for the dielectric measurements was set to 1 and 4 GHz, respectively. This range was chosen as it is the relevant frequency range for microwave tomography studies[23]. The probe operates between 0.5–50 GHz and needs a minimum of 5 mm sample thickness for measurements. The ideal measurement requires the immersion of the probe into an isotropic medium. The network analyser measures the reflection coefficient of the material under test, not its dielectric constant. The software, through a model, translates the reflection coefficient to complex dielectric constant values, which captures the permittivity and conductivity of the material via the frequency

dependent equation;

$$\epsilon^*(\omega) = \epsilon^{'}(\omega) - j\epsilon^{''}(\omega) = \epsilon^{'}(\omega) - j\frac{\sigma}{\omega\epsilon_0} \tag{1}$$

Equation (1) refers to the frequency dependent complex dielectric constant $\epsilon^*(\omega)$, which is equal to the real part (dielectric constant) $\epsilon'(\omega)$, the imaginary part $\epsilon''(\omega)$ ($j = \sqrt{-1}$), which in turn is related to the effective conductivity (σ) of the material at specific frequencies. The angular frequency is represented by ω and ϵ_0 is the dielectric constant of free space. It is notable that the real part decreases and the imaginary part increases with respect to frequency in the microwave region[24].

IV. RESULTS

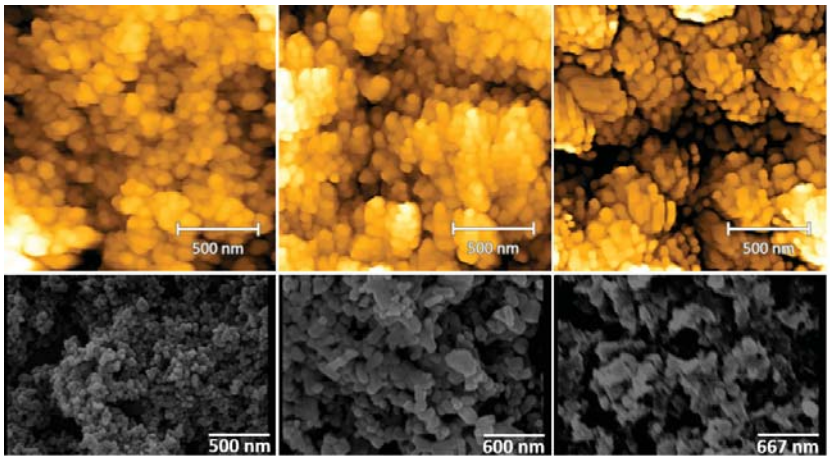

FIG. 1. The surface morphology is observed from AFM and SEM. AFM images of SiO_2 (top left), ZnO (top middle) and ZnO-PEG (top right). SEM images of SiO_2 (bottom left with a scale of 500 nm), ZnO (bottom middle with a scale of 600 nm) and ZnO-PEG (bottom right with a scale of 667 nm). Images were taken at room temperature. SEM images were taken in a vacuum environment, while the AFM images were taken in open air conditions.

A. Nanoparticle characterisation using AFM, SEM, UV-Vis and DLS

We have characterised the surface morphology of SiO_2, ZnO and ZnO-PEG by AFM and SEM (FIG. 1). Analysis for AFM confirmed the averaged particle size (diameter) of

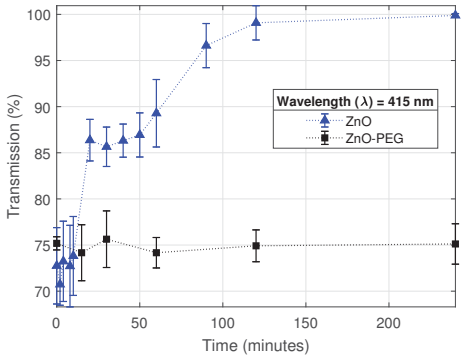

(a) UV-Vis spectra

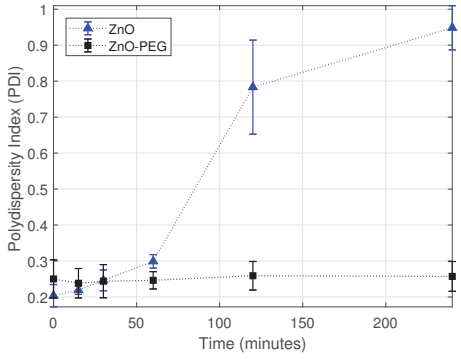

(b) PDI (DLS)

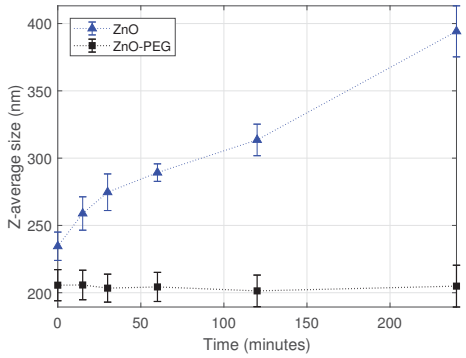

(c) Z-average size (DLS)

FIG. 2. The following plots show the stability of basic and modified ZnO; (a) Light transmission through ZnO NP and ZnO-PEG (M_W=8000) dispersed in RO water taken at a wavelength (λ) of 415 nm, (b) plots of the average polydispersity index (PDI) and (c) Z-average size (nm) of ZnO and ZnO-PEG NPs dispersed in RO water over a time period of 4 hours with a sample population of 6 elements.

240 51.58 ± 4.72 nm, 53.2 ± 10.7 nm and 65.65 ± 6.02 nm for ZnO, SiO_2 and ZnO-PEG respectively. SEM suggests an average size of 59.6 ± 3.5 nm, 14.33 ± 12.7 nm and 91.1 ± 8.7 nm for ZnO, SiO_2 and ZnO-PEG respectively. The shape of all the NPs are shown to be spherical in nature, although they are highly varied in sizes. FIG. 2(a) shows the UV-Vis 245 transmission spectra of ZnO and ZnO-PEG NP dispersions. Measurements were taken at a final concentration of 10 μg/mL and at a wavelength of 415 nm. The measurements for ZnO-PEG were taken at an interval of 15 minutes. Results suggest that the transmission of light through unmodified ZnO NP dispersion increases rapidly after 30 minutes and continues to increase to 100 % in most samples within 2 hours, suggesting sedimentation of the ZnO

NPs. Also, this was observed visually due to the apparent precipitation of the NPs. ZnO-PEG showed an initial transmission of $\sim$ 75 %, and they were found to have a similar transmission over a 4 hour period; suggesting dispersion of ZnO NPs is better and stable after PEGylation.

Dynamic light scattering measurements (FIG. 2(b) & FIG. 2(c)) of ZnO and ZnO-PEG in solution were carried out to characterise the intensity weighted Z-average size and polydispersity index (PDI). The mean particle size is very specific to light scattering and to the presence of NP aggregates. Values of PDI ranges from 0 to 1; a PDI value smaller than 0.1 shows the sample is nearly monodisperse, while a PDI equal to 1 indicates the sample has a large variation in particle size. PDI of ZnO-PEG remains to be around 0.25 and stays constant throughout 4 hours. However, the PDI for ZnO NPs increases from 0.2 to 0.95 within the measurement period. High PDI suggests a broad distribution of particle sizes and presence of large aggregates. The Z-average size of ZnO increases from $\sim$ 240 nm to $\sim$ 400 nm compared to ZnO-PEG which has a constant size of $\sim$ 210 nm throughout 240 minutes. This suggests that aggregation of the ZnO NPs is reduced after the PEGylation process and the particles were stable. Stability studies for SiO_2 and CNT-OH were not included, as they were only used as controls and main focus of this paper is on ZnO and ZnO-PEG NPs.

B. Microwave properties of nanoparticle suspensions

FIG. 3(a) shows the measured dielectric properties of single-walled carbon nanotubes functionalised with hydroxyl group (CNT-OH) dispersed in RO water. The dielectric constant shows a dependency on the concentration of NPs in the MUT. The maximum change in the effective conductivity (FIG. 4(a)) observed by CNT-OH was 42.63 % and dielectric constant showed a 10.61 % increase from the background medium at 1 GHz. The variation of measurements at 2 mg/mL (max $\sigma_{std} = \pm 2.47$) is considerably higher compared to lower concentrations, which may be due to the instability and aggregation of the NPs at higher concentrations. Instability of the NPs at higher concentration is likely because, as the concentration increases, interparticle distances decrease, hence leading to higher collision and aggregation of NPs. FIG. 3(b) displays the dielectric constant of silicon dioxide dispersed in RO water with 1 % (v/v) Pluronic surfactant at different concentrations. The maximum $\epsilon'(\omega)$ value is 80.91 (f = 1.27 GHz), 81.18 (f = 1.12 GHz), 81.27 (f = 1.12 GHz), 81.26 (f =

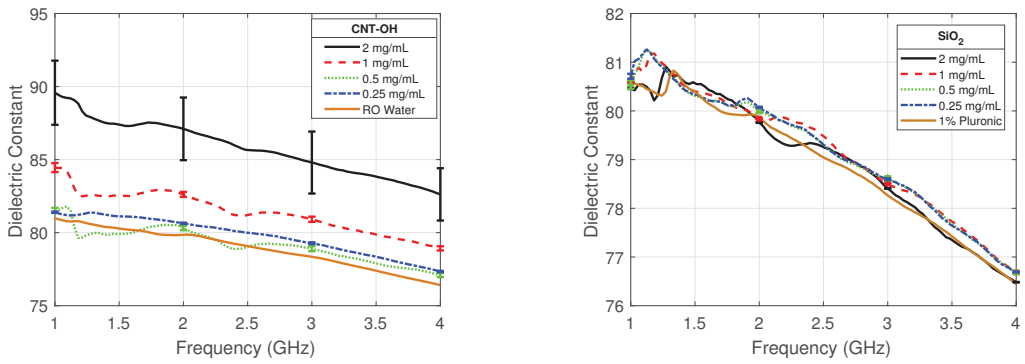

(a) CNT-OH (RO Water)

(b) SiO_2 (1% Pluronic)

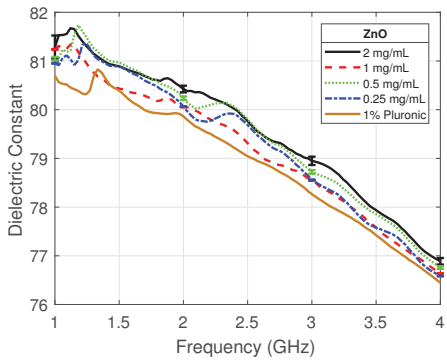

(c) ZnO (1% Pluronic)

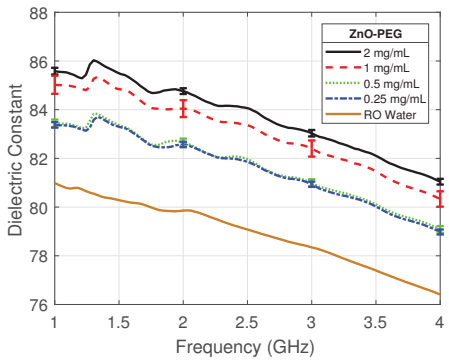

(d) ZnO-PEG (RO Water)

FIG. 3. Average dielectric constant of colloidal dispersions of (a) CNT-OH in RO water, (b) SiO_2 with 1 % Pluronic, (c) ZnO with 1 % Pluronic, and (d) ZnO-PEG in RO water characterised between 1–4 GHz.

1.12 GHz), in descending order of SiO_2 concentration. The maximum value of 1 % Pluronic in water is 80.3 recorded at 1.33 GHz. FIG. 4(b) shows no change in the conductivity of the dispersions. The average change of the dielectric constant of SiO_2 NPs with respect to the background is less than 1.5 % below 2 GHz.

FIG. 3(c) & FIG. 4(c) show the dielectric and conductivity properties of zinc oxide NPs from a frequency range of 1 to 4 GHz. Dielectric constant of ZnO at 2 mg/mL at 1 GHz is 81.28 ± 0.24 with 0.73 % change to water compared to 80.95 ± 0.01 with 0.32 % change of the 0.25 mg/mL concentration. Therefore, the concentration dependence is visible. FIG. 3(d) shows the dielectric constant of ZnO-PEG NPs. It is evident that increase in the ZnO-PEG concentration is directly proportional to the increase in the dielectric constant over the whole frequency range. The maximum average change of $\epsilon'(\omega)$ of ZnO NPs at 2, 1, 0.5,

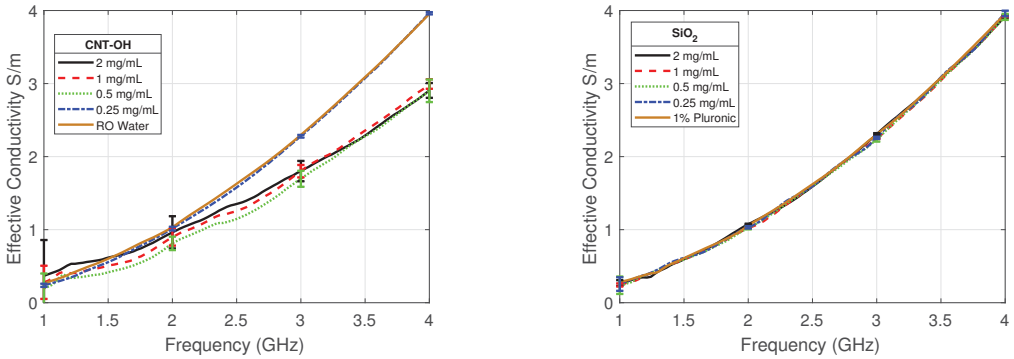

(a) CNT-OH (RO Water)

(b) SiO_2 (1% Pluronic)

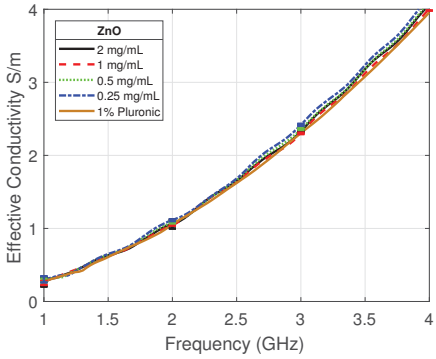

(c) ZnO (1% Pluronic)

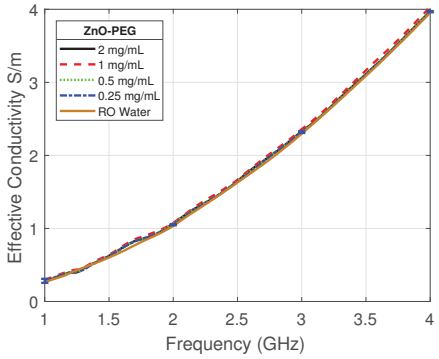

(d) ZnO-PEG (RO Water)

FIG. 4. Average effective conductivity of colloidal dispersions of (a) CNT-OH in RO water, (b) SiO_2 with 1 % Pluronic, (c) ZnO with 1 % Pluronic, and (d) ZnO-PEG in RO water characterised between 1–4 GHz.

and 0.25 mg/mL is 1.99 %, 1.58 %, 2.11 % and 1.70 %, respectively. The average change of PEGylated zinc oxide NPs (FIG. 5(b)) in 2, 1, 0.5, and 0.25 mg/mL is 6.80 %, 6.03 %, 4.14 % and 4.00 % accordingly, at 1 GHz. From FIG. 5(a), CNT-OH at 2 mg/mL concentration shows the highest average change in dielectric constant, however at lower concentrations, ZnO-PEG shows higher average change compared to CNT-OH.

Furthermore, we measured the dielectric properties of our colloidal dispersions at higher frequencies (Supplementary material; Section A; Table S1). The purpose of characterising at high frequencies was to identify if a similar impact of these NPs on the dielectric contrast is equally observed at higher frequencies, and to what extent. Our results showed, that average change of ZnO colloidal suspension across a wide frequency range remains to be ∼2%, which is what we observed at lower frequency range and SiO_2 remains to have similar

dielectric properties to that of water with 1% Pluronic as observed at lower frequency range. With regards to ZnO-PEG the overall average change remains to be ∼6%, and slightly changed depending on the frequency points. However, the results are similar to that of lower frequency range. Average change for CNT-OH across the large frequency range remains to be the highest amongst the different nanomaterials we measured.

V. DISCUSSION

A. Morphology and stability analysis

Satisfactory agreement is shown between the size and the shape of AFM and SEM morphology characterisation for ZnO, SiO_2 and ZnO-PEG. Modified zinc oxide has much larger size compared with basic ZnO, suggesting PEGylation has been effective. The shape of all the NPs are represented as spherical in SEM and AFM.

The purpose of carrying out light transmission studies was to investigate the stability of colloidal dispersions. PEGylated ZnO NPs are more stable compared to non-PEGylated ZnO NPs (FIG. 2(a)). Non-PEGylated ZnO NPs are likely to aggregate in a solution and then sediment within the cuvette increasing the light transmission. The process of vortexing and sonication was carried out to ensure a homogenous solution. Colloidal stability is important for a homogenous aqueous dispersion during dielectric measurements, and it is crucial in improving NP dispersions in physiological conditions such as blood.

Z-average size generated from the DLS differs greatly from the AFM and SEM particle size. By using this technique, we were able to measure the size of the NPs when dispersed in a solution. Z-average size is an intensity weighted mean particle diameter, which is relevant to scattering of light and is sensitive to large aggregates, due to its inherent intensity weighting and dependency on viscosity and temperature. It presents the size of a spherical particle that has equal diffusion as the particle in question. The diffusion of the particles in solution will also depend on the conformation of the PEG attached. Large PEG chains, such as the ones used in this study may be described by the Flory radius equation (2), F is the Flory radius, α is the length of a single monomer repeat and n (n = $(M_W)/44$) is the number of monomers on the PEG chain itself[25]; the Flory radius for PEG 8000 is 79.4 nm.

$$F = \alpha n^{\frac{3}{5}} \tag{2}$$

The distance between the NP surface and the PEG may induce a brush or mushroom conformation[26]. If F is smaller than the distance between the surface and the PEG chain, then a mushroom conformation occurs, however if F is larger than the surface density then it would lead to a brush conformation. The ionic concentration of the samples was minimal, therefore the electrical Debye length ($\kappa^{(-1)}$) around the particle would be extended, reducing the diffusion speed, hence a larger hydrodynamic size would be present.

B. Dielectric analysis

We have measured the dielectric properties of selected nanomaterials to assess contrast enhancing properties in high dielectric constant media. We aim to identify simple dielectric parameters so we can extrapolate and compare nanomaterials. The desired contrast should be visible in the real part of the complex dielectric constant rather than the imaginary part. Increase in the conductivity may cause increase in dielectric losses, hence being unreliable for imaging purposes[27]. Microwave reflection measurements (S11) using the coaxial probe are susceptible to systematic errors, which causes the jitter in the frequency dispersion, especially at low frequencies. To minimize this error, repeated calibrations were performed and observation of the polar plot for each calibration standard was inspected as a confidence check. Moreover the contrast observed has to be larger than the stated 2 % error of the probe[28]. Generally, the complex dielectric constant may depend on temperature as well as frequency, and increase in the temperature of water will increase the loss index and therefore decrease dielectric constant[29].

The measurements of the dielectric properties of colloidal dispersions could be influenced by aggregation and precipitation phenomena. The probe's stated sensing depth is 5 mm; however, the actual sensing volume is experimentally much smaller. 90 % of the overall dielectric property of a mixture is dependent on the initial 500 μm from the tip of the probe length[30]. Also, the probe assumes that the sample is isotropic and non-magnetic.

Dielectric isotropy may be dependent on the homogeneity of the tested nanomaterials dispersed in their respective solvents. Moreover, we have mentioned that the probe measurements are limited to a small measurement depth. To assess the effect of colloidal stability

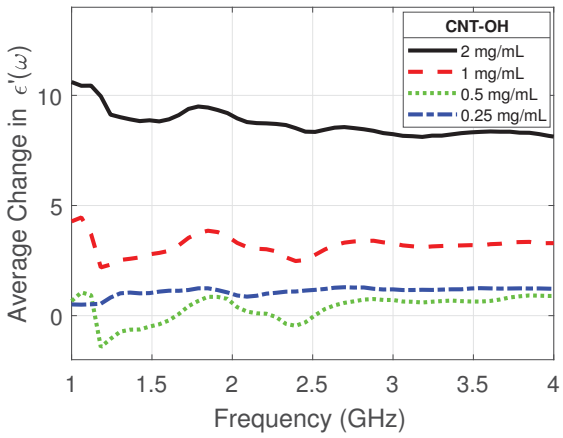

(a) CNT-OH (RO Water)

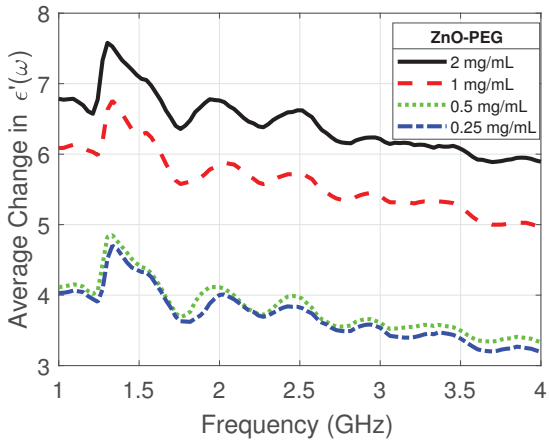

(b) ZnO-PEG (RO Water)

FIG. 5. Average change of the dielectric constant of colloidal dispersions of (a) CNT-OH and (b) ZnO-PEG in aqueous solution from 1–4 GHz.

of NPs on their dielectric properties that could be affected by probe distance, we measured the properties at three different probe positions. We observed that the measurements of the suspensions, such as the ZnO, SiO_2, ZnO-PEG and CNT-OH were very similar at different positions over 25 minutes (Supplementary material; Section B; FIG. S1 - S4).

1. Evaluation of nanoparticle colloidal dispersions

Previously CNTs have been extensively explored as potential contrast agents for MWI due to their distinctive electrical properties. The purpose of measuring CNTs was to use them

as a control since they have been previously suggested as effective contrast agents. Results obtained for CNT-OH correlate positively with previously reported data. It's important to note that OH functionalized CNTs showed an average change of 10.61 % increase in the real component at 2 mg/mL at 1 GHz, which is comparable with previously reported (CNTs stabilised with biocompatible PL-PEG) 10 % increase in the dielectric constant and 90 % increase in conductivity at similar conditions[11]. However, we only observed an increase of 42.63 % in the conductivity, similar to [13].

Carbon atoms in a CNT structure are known to be arranged in a hexagonal lattice, where each carbon atom is covalently bonded to three neighbouring carbons via sp^2 molecular orbitals. The fourth valence electron remains empty and delocalized, hence making CNTs conductive in nature[31]. CNTs have been reported to have a high aspect ratio, which has been stated to increase the dielectric constant due to the presence of a large dipole moment[32]. When an alternating electric field is applied, the hydroxyl group in CNT would experience orientational polarisation[33], which leads to a torque acting on the polar -OH bond. The torque prompts the nanotubes to orient along the electric field, hence an increase in the dielectric constant is observed[34].

However, biocompatibility of CNTs is in question, which further motivated us to study other nanomaterials for their potential as contrast agents for MWI. CNTs may have adverse effects on human health, especially in human pulmonary system[35]. It is understood that surface modifications are important to minimise CNT toxicity[36].

The suspension of silicon dioxide NPs in water shows a negligible change in the dielectric constant over the whole frequency range compared to zinc oxide NPs and CNT-OH. Silicon dioxide is not conductive and has no net dipole due to its crystalline structure. Silicon dioxide has a tetrahedral arrangement of four sp^3 hybrid orbitals[37]. In a silicon-oxygen tetrahedra, each silicon atom is surrounded by four oxygen atoms[38]. The individual Si-O bonds are very polar but there are four Si-O bond which cancels each other out, hence there is no net dipole effect.

One of the key features of ZnO NPs is their low toxicity and biodegradability. It is involved in various aspects of metabolism. Numerous studies have shown the biocompatibility and biosafety of ZnO nanostructures when applied in biological applications[39, 40]. ZnO has particular electrical properties such as they are known to have a wide band gap energy (3.4 eV), large exciton binding energies (60 meV), and they have a structure of alternating planes

composed of tetrahedral coordinated O^{2-} and Zn^{2+} ions[41]. This results in non-central symmetric structure[42] and consequently piezoelectric and pyro-electric behaviour[43, 44]. Zinc oxide has polar surfaces at the positive Zn-(0001) and the negative O-(0001) surfaces, resulting in a normal dipole moment[45, 46]. The opposing charged ions produce a polar surface, which leads to the formation of a dipole moment and spontaneous polarisation when an electric field is applied, hence increase in the dielectric constant with ZnO NPs is possible.

2. Impact of PEGylation on dielectric constant

Colloidal solutions tend to lower their stability because of particle size and free surface energy[47]. Nanoparticles stabilise themselves either by sorption of molecules from their surroundings or by lowering their surface area through coagulation and agglomeration[48]. Homogenous solution was obtained at lower concentrations, however particles were still unstable and higher concentrations caused sedimentation. Since, ZnO NPs showed a potential increase in the dielectric constant, they were PEGylated to further improve their stability in the solution and to confirm the effect dispersion has on the dielectric properties.

Polyethylene glycol is a chemically inert molecule of varying lengths[49], making it a good dispersant in water. PEGylation provides hydrophilicity to the NPs by making them water dispersible. PEG can be attached onto the surface of NPs via adsorption; hydrophobic interactions, through the formation of covalent bonds or hydrogen bonding[50]. PEG is adsorbed onto the ZnO particle surface and then attains the adsorption plateau. The total amount of PEG adsorbed is larger for larger molecular weights due to greater participation of loop and tail segment at the surface. The type (-$ZnOH_2^+$, -ZnOH, -ZnO^-) and number of surface groups on ZnO NPs may determine the extent of polymer adsorption[51]. The dispersion of ZnO NPs was improved after PEGylation as shown by the UV-Vis (FIG. 2(a)) and by DLS (FIG. 2(b) & FIG. 2(c)). We further improved the dielectric properties of ZnO NPs after PEGylation, suggesting the importance of a homogenous and a stable solution. However, ZnO-PEG NPs in water show a non-linear concentration dependent change in the dielectric constant. This might be because a minimum nanomaterial concentration is required to provide a significant contrast, below which dielectric probe measurements are not reliable.

Comparable results were obtained for CNTs by Song *et al.*[52]. The authors found similar effective conductivities for 0.22 and 0.5 % (w/v) but significantly higher for 1 % (w/v) CNT

dispersions. However, Mashal *et al.* (2010) used SWCNTs at three concentrations in tissue-mimicking phantoms and they observed a better concentration dependent increase though not a clear linear increase. The authors used an oil-gelatin phantom which could promote better SWCNTs dispersion (less Brownian motion) compared to water.

We would like to highlight, that dielectric properties of NPs in liquid solutions do not exhibit a linear dependence with their concentrations in water. This may be due to following reasons: at low concentrations, the effect of NPs may be very low to be distinguishable within the error of the probe measurement, such as with the case of ZnO-PEG (and other) NPs. At higher concentrations, dispersion of the NPs in the liquids may be less effective as their concentration increases, hence it is possible that a concentration increase from 0.5 to 1.0 mg/mL has a stronger impact on the dielectric properties of the liquid solution than an increase from 1.0 to 2.0 mg/mL, as seen in FIG.5.

We note that in future experimental studies, such as *in-vitro/in-vivo*, dosage of NPs and concentrations will have to be addressed. We also aim to use different tumour targeting techniques that will increase the concentration of NPs in a tumour. Receptor targeting of NPs using chemically anchored ligands/antibodies and hyperthermia are tested methods to increase NP concentration in solid tumours. These tools will be used in combination with a suitable nanomaterial for MWI. However, selection of such nanomaterial will require full investigation of dielectric properties in water, tissue-mimicking phantoms, homogenated tissues before optimisation for *in-vivo* purposes. The time required for the accumulation of NPs is important and depends on various factors, such as, bio distribution, blood clearance and the rate of accumulation of NPs in tumours post intravenous injection. Parameters that require elucidation are the minimum concentration of contrast agents per tissue volume to give a significant microwave signal and the concentrations that may maximise contrast assessed by MWI. Using other imaging modalities (e.g. optical imaging), we note that the time that is necessary for labelled NPs to give a minimum and maximum signal in tumours in mice occurs at one and five hours, respectively after intravenous administration[53]. Using MRI (magnetic resonance imaging) and modified iron oxide NPs the values for minimum and maximum signals in tumours post administration are 1h and 3h respectively[54]. We would expect similar accumulation time for MWI contrast enhancing agents.

VI. CONCLUSION

We investigated the dielectric properties of nanomaterials in a frequency range between 1–4 GHz. We have demonstrated that zinc oxide NPs have the potential of producing a difference within the dielectric properties when dispersed in high dielectric constant medium i.e. water. We suggest that this difference is observed with zinc oxide NPs because it possess polar surfaces. It can also be concluded from this study that dispersion plays a key role when taking dielectric measurements. We could see an increase within the dielectric properties of ZnO in water after they had been PEGylated because of colloidal stability. The ZnO-PEG NPs increase the dielectric properties of the medium in a concentration dependent manner that is non-linear.

The paper's results motivate further *in-vitro* and *in-vivo* investigation of ZnO-PEG NPs as potential contrast agents for MWI, to define their impact on the tumour's dielectric properties. If this impact is significant, ZnO-PEG NPs will be developed for tumour targeting using ligand as receptors on cancer cells. We envision two possible routes for microwave breast cancer detection using these NPs. The first approach would apply microwave tomography algorithms to reconstruct the breast interior before and after injecting the NPs and produce a differential image, as shown with simulations[55]. The second approach would operate directly on the differential signals acquired before and after the agents injection, using radar-based methods to detect and localize the contrast-enhanced tumour area[56].

[1] S. Kwon and S. Lee, International Journal of Biomedical Imaging **2016**, 1 (2016).

[2] H. D. Trefná, J. Vrba, and M. Persson, International Journal of Hyperthermia **26**, 185 (2010).

[3] P. Wust, B. Hildebrandt, G. Sreenivasa, B. Rau, J. Gellermann, H. Riess, R. Felix, and P. Schlag, The Lancet Oncology **3**, 487 (2002).

[4] D. Andreuccetti, R. Fossi, and C. Petrucci, "An internet resource for the calculation of the dielectric properties of body tissues in the frequency range 10 Hz - 100 GHz," (1997), based on data published by C.Gabriel et al. in 1996.

[5] R. Pethig, Clinical Physics and Physiological Measurement **8**, 5 (1987).

[6] W. T. Joines, Y. Zhang, C. Li, and R. L. Jirtle, Medical Physics **21**, 547 (1994).

[7] M. Lazebnik, L. McCartney, D. Popovic, C. B. Watkins, M. J. Lindstrom, J. Harter, S. Sewall,

A. Magliocco, J. H. Booske, M. Okoniewski, and S. C. Hagness, Physics in Medicine and Biology **52**, 2637 (2007).

[8] M. Lazebnik, D. Popovic, L. McCartney, C. B. Watkins, M. J. Lindstrom, J. Harter, S. Sewall, T. Ogilvie, A. Magliocco, T. M. Breslin, W. Temple, D. Mew, J. H. Booske, M. Okoniewski, and S. C. Hagness, Physics in Medicine and Biology **52**, 6093 (2007).

[9] H. Maeda, J. Wu, T. Sawa, Y. Matsumura, and K. Hori, Journal of Controlled Release **65**, 271 (2000).

[10] O. Ogunlade and P. Beard, Medical Physics **42**, 170 (2015).

[11] X. Li, A. V. Sahakian, S. C. Hagness, and J. H. Booske, *Nanoparticle Contrast Agents for Enhanced Microwave Imaging and Thermal Treatment of Breast Cancer*, Tech. Rep. (Northwestern University, 2010).

[12] S. X. Xie, F. Gao, S. C. Patel, J. H. Booske, S. C. Hagness, and B. Sitharaman, IEEE Transactions on Biomedical Engineering **61**, 2718 (2014).

[13] S. X. Xie, F. Gao, S. C. Patel, J. H. Booske, S. C. Hagness, and B. Sitharaman, Applied Physics Letters **103**, 133114 (2013).

[14] A. Mashal, B. Sitharaman, X. Li, P. K. Avti, A. V. Sahakian, J. H. Booske, and S. C. Hagness, IEEE Transactions on Biomedical Engineering **57**, 1831 (2010).

[15] A. Mashal, J. H. Booske, and S. C. Hagness, Physics in Medicine and Biology **54**, 641 (2009).

[16] G. Bellizzi, O. M. Bucci, I. Catapano, L. Crocco, and R. Scapaticci, in *Proceedings of the 2012 IEEE International Symposium on Antennas and Propagation* (2012) pp. 1–2.

[17] O. M. Bucci, G. Bellizzi, A. Borgia, S. Costanzo, L. Crocco, G. D. Massa, and R. Scapaticci, in *2016 10th European Conference on Antennas and Propagation (EuCAP)* (2016) pp. 1–4.

[18] G. Bellizzi and O. M. Bucci, IEEE Transactions on Magnetics **49**, 2903 (2013).

[19] O. M. Bucci, G. Bellizzi, and G. G. Bellizzi, IEEE Transactions on Magnetics **53**, 1 (2017).

[20] M. W. Rahman, R. Lahri, M. Wright, M. Koutsoupidou, T. Kallos, M. Thanou, and P. Kosmas, in *2017 International Conference on Electromagnetics in Advanced Applications (ICEAA)* (2017) pp. 1021–1024.

[21] M. Tshabalala, B. Dejene, and H. Swart, Physica B: Condensed Matter **407**, 1668 (2012).

[22] Keysight, *Keysight 85070E Dielectric Probe Kit 200 MHz to 50 GHz Technical Overview* (2014).

[23] Z. Miao and P. Kosmas, IEEE Transactions on Antennas and Propagation **65**, 2507 (2017).

[24] A. V. Vorst, A. Rosen, and Y. Kotsuka, "RF/microwave interaction with biological tissues," (Wiley-IEEE Press, 2006) Chap. Fundamentals of Electromagnetics, pp. 7–54.

[25] J. V. Jokerst, T. Lobovkina, R. N. Zare, and S. S. Gambhir, Nanomedicine **6**, 715 (2011).

[26] H. Lee, A. H. de Vries, S.-J. Marrink, and R. W. Pastor, The Journal of Physical Chemistry B **113**, 13186 (2009).

[27] P. M. Meaney, S. A. Pendergrass, M. W. Fanning, and K. D. Paulsen, Journal of Electromagnetic Waves and Applications **17**, 333 (2003).

[28] Agilent, *85070E Dielectric Probe Kit Help File* (2013).

[29] U. Kaatze, Journal of Chemical & Engineering Data **34**, 371 (1989).

[30] P. M. Meaney, A. P. Gregory, N. R. Epstein, and K. D. Paulsen, BMC Medical Physics **14**, 1 (2014).

[31] V. N. Popov, Materials Science and Engineering: R: Reports **43**, 61 (2004).

[32] H. Tang, Z. Zhou, and H. A. Sodano, ACS Applied Materials & Interfaces **6**, 5450 (2014).

[33] A. Das, S. Sinha, A. Mukherjee, and A. Meikap, Materials Chemistry and Physics **167**, 286 (2015).

[34] Y. Bao, H. Pang, L. Xu, C.-H. Cui, X. Jiang, D.-X. Yan, and Z.-M. Li, RSC Advances **3**, 24185 (2013).

[35] C. Lam, J. T. James, R. McCluskey, S. Arepalli, and R. L. Hunter, Critical Reviews in Toxicology **36**, 189 (2006).

[36] I. Fenoglio, G. Greco, M. Tomatis, J. Muller, E. Raymundo-Piñero, F. Béguin, A. Fonseca, J. B. Nagy, D. Lison, and B. Fubini, Chemical Research in Toxicology **21**, 1690 (2008).

[37] W. McPherson and W. E. Henderson, "An elementary study of chemistry," (Ginn and Company, 1905) Chap. Silicon, Titanium, Boron, pp. 257–266.

[38] IARC, "Silica, some silicates, coal dust and para-aramid fibril," (IARC, 1997) Chap. Silica.

[39] C. Hanley, J. Layne, A. Punnoose, K. M. Reddy, I. Coombs, A. Coombs, K. Feris, and D. Wingett, Nanotechnology **19**, 295103 (2008).

[40] Z. Li, R. Yang, M. Yu, F. Bai, C. Li, and Z. L. Wang, The Journal of Physical Chemistry C **112**, 2011420117 (2008).

[41] A. Iglesias-Juez, F. Vines, O. Lamiel-Garcia, M. Fernandez-Garcia, and F. Illas, Journal of Materials Chemistry A **3**, 8782 (2015).

[42] V. E. Henrich and P. A. Cox, "The surface science of metal oxides," (Cambridge University

Press, 1996) Chap. Wurtzite, pp. 55–59.

[43] Z. L. Wang, Journal of Physics: Condensed Matter **16**, R829R858 (2004).

[44] C. Vidyasagar and Y. A. Naik, Arabian Journal of Chemistry **9**, 507 (2016).

[45] O. Dulub, U. Diebold, and G. Kresse, Physical Review Letters **90**, 016102 (2003).

[46] O. Dulub, L. A. Boatner, and U. Diebold, Surface Science **519**, 201 (2002).

[47] A. Ali, H. Zafar, M. Zia, I. ul Haq, A. R. Phull, J. S. Ali, and A. Hussain, Nanotechnology, Science and Application **9**, 49 (2016).

[48] J. Polte, CrystEngComm **17**, 6809 (2015).

[49] J. Chen, S. K. Spear, J. G. Huddleston, and R. D. Rogers, Green Chemistry **7**, 64 (2005).

[50] S. Liufu, H. Xiao, and Y. Li, Powder Technology **145**, 20 (2004).

[51] G. Nabiyouni, A. Barati, and M. Saadat, Iranian Journal of Chemical Engineering **8**, 20 (2011).

[52] J. Song, Z. Zhao, J. Wang, X. Zhu, J. Wu, Z. Nie, and Q. H. Liu, IEEE Transactions on Biomedical Engineering **62**, 930 (2015).

[53] E. V. Rosca, M. Wright, R. Gonitel, W. Gedroyc, A. D. Miller, and M. Thanou, Molecular Pharmaceutics **12**, 1335 (2015).

[54] Y. Lv, P. Chandrasekharan, Y. Li, X.-L. Liu, J. Penaranda-Avila, Y. Yang, K.-H. Chuang, X.-J. Liang, and J. Ding, Journal of Materials Chemistry B (2018).

[55] J. D. Shea, P. Kosmas, B. D. V. Veen, and S. C. Hagness, Inverse Problems **26**, 074009 (2010).

[56] Y. Chen and P. Kosmas, IEEE Transactions on Biomedical Engineering **59**, 766 (2012).